NRC Research Press

ARTICLE

Natural convection in a triangular cavity filled with a nanofluid-saturated porous medium using three heat equation model

Mahmoud Sabour and Mohammad Ghalambaz

Abstract: The present study aims to examine the local thermal non-equilibrium natural convection heat and mass transfer of nanofluids in a triangular enclosure filled with a porous medium. The effect of the presence of nanoparticles and the thermal interaction between phases on the flow, temperature distribution of phases, the concentration distribution of nanoparticles as well as the Nusselt number of phases is theoretically studied. The interaction between the phases of nanoparticles and the base is taken into account by using a three thermal energy equation model while the concentration distribution of nanoparticles is modeled by Buongiorno's model. A hot flush element is mounted at the vertical wall of the triangle enclosure to provide a constant temperature of T_h while the inclined wall is at a constant temperature of T_c. A three heat equation model by considering the local thermal non-equilibrium model of nanoparticles, the porous medium, and the base fluid is developed and utilized for natural convection of nanofluids in an enclosure. The drift-flux of nanoparticles due to the nano-scale effects of thermophoresis and Brownian motion effects is addressed. The governing equations are represented in a non-dimensional form and solved by employing the finite element method. The results indicate that the increase of Rayleigh number shows a significant increase in the average Nusselt number for the base fluid phase, a less significant increase in the average Nusselt number for the solid matrix phase, and almost an insignificant effect in the average Nusselt number of the nanoparticle phase. Increasing the buoyancy ratio parameter (the ratio of mass transfer buoyancy forces to the thermal buoyancy forces) tends to reduce and increase the average Nusselt number in fluid and porous phases, respectively. An optimum value of buoyancy ratio parameter for the average Nusselt number of the nanoparticle phase is observed.

Key words: nanofluid-saturated porous media, thermal non-equilibrium model, buongiorno model, thermophoresis, natural convection.

Résumé : Nous examinons ici le transfert de chaleur et de masse par convexion naturelle sans équilibre thermique local, dans une enceinte triangulaire remplie d'un médium poreux. Nous faisons une étude théorique des effets de la présence de nanoparticules et de l'interaction thermique entre les phases, sur l'écoulement, la distribution de température des phases, la distribution de concentration des nanoparticules et du nombre de Nusselt des phases. Nous tenons compte de l'interaction entre les phases de nanoparticules et la base en utilisant une équation modèle à trois énergies thermiques, alors que la distribution de concentration des nanoparticules est modélisée par le modèle de Buongiorno. Un élément chauffant est monté au mur vertical de l'enceinte triangulaire afin d'y garantir une température constante T_h, alors que le mur incliné est à température constante T_c. Une équation modèle à trois chaleurs est développée en considérant un modèle de non équilibre thermique local des nanoparticules, du médium poreux et du fluide de base et est utilisée pour la convexion naturelle de nano-fluides dans l'enceinte. Nous abordons la dérive de flux de nanoparticules due aux effets à nano-échelle des effets de thermophorèse et de mouvement Brownien. Les équations directrices sont représentées sous forme sans dimension et solutionnées par méthode d'éléments finis. Les résultats montrent que l'augmentation du nombre de Rayleigh indique une augmentation significative de la valeur moyenne du nombre de Nusselt pour le fluide de base, une augmentation moins importante du nombre de Nusselt pour la matrice solide et pratiquement aucun effet pour le nombre de Nusselt pour la phase nanoparticule. L'augmentation du rapport de flottabilité (le rapport des forces de flottabilité de transfert de masse aux forces de flottabilité thermique) tend à réduire et à augmenter le nombre moyen de Nusselt des phases poreuse et nanoparticule respectivement. Nous observons une valeur optimale du rapport de flottabilité pour le nombre moyen de Nusselt de la phase nanoparticule. [Traduit par la Rédaction]

Mots-clés : médium poreux saturé de nanoparticules, modèle de non équilibre thermique, modèle de Buongiorno, thermophorèse, convexion naturelle.

PACS Nos.: 44.30.+v, 44.25.+f.

1. Introduction

The flow and heat transfer in porous media is the subject of many industrial applications, such as flow through grains, fibers, or compact heat exchangers. In many engineering and physical applications of convective heat transfer in porous media, it could be assumed that the interaction between the fluid and the porous matrix is very high, and hence, the temperature difference between the flowing fluid and the porous medium material is negligible. In this case, the energy of the fluid and porous medium can be represent by an affective heat equation for the mixture of

Received 24 January 2016. Accepted 28 March 2016.

M. Sabour and M. Ghalambaz. Department of Mechanical Engineering, Dezful Branch, Islamic Azad University, Dezful, Iran.
Corresponding author: Mohammad Ghalambaz (email: m.ghalambaz@iaud.ac.ir).

the fluid and porous medium. This model is known as the local thermal equilibrium model.

There are many research studies in the literature that have examined free convective heat transfer in porous enclosures, using the local thermal equilibrium model. For example, Baytas and Pop [1], Saeid and Pop [2], Basak et al. [3, 4], Sathiyamoorthy et al. [5], Chamkha and Ismael [6], and Chamkha and Ismael [7] studied different aspects of convective heat transfer in porous media utilizing the local thermal equilibrium model. However, there are many practical cases in which the thermal equilibrium model between the phases is not valid, and the temperature of the phases is quite distinct. In these situations, local thermal non-equilibrium models are required.

The local thermal non-equilibrium free convective heat transfer for regular fluid has found very important practical engineering applications in thermal removal systems and petroleum applications. For example, a highly conductive heat sink for cooling of high power electronic devices or nuclear fuel rods in a cooling bath can be modeled by the local thermal non-equilibrium model of porous media. There are some excellent studies considering the local thermal non-equilibrium models for convective heat transfer of fluids in porous media [8–10].

Recently, nanofluids and high conductive metallic porous foams have been proposed as potential media to enhance the heat transfer for applications in heat removal systems. Nanofluids have been proposed as new engineered fluids with enhanced thermophysical properties to increase the convective heat transfer potential of conventional heat transfer fluids [11–14]. Heat transfer potential of nanofluids has been examined in many recent studies [15–19]. In the case of metallic porous foams, as the thermal conductivity of porous foams is high, the temperature difference between the porous matrix and the free convective flow of the fluid could be important. Hence, in analysis of such systems, considering local thermal non-equilibrium models is very important.

The free convective heat transfer of nanofluids in enclosures, saturated with porous media, has been studied recently. For instance, Sun and Pop [20] studied the free convective heat transfer of nanofluids in a triangular cavity by considering the local thermal equilibrium among the phases of nanoparticles, porous matrix and the base fluid. Sheremet et al. [21, 22] studied the convective heat transfer of nanofluids in a square cavity filled with a nanofluid by using Tiwari and Das's nanofluid model. Tiwari and Das's nanofluid model assumes a homogeneous distribution of nanoparticles in the base fluid and porous media. The Tiwari and Das nanofluid model was also utilized by Ghalambaz et al. [23] to study the free convective heat transfer of nanofluids in a parallelogrammic porous cavity filled with a porous medium.

Sheremet and Pop [24] investigated the free convective heat transfer of nanofluids in a square cavity by using Buongiorno's mathematical model [25]. Buongiorno's mathematical model [25] evaluates the concentration distribution of nanoparticles due to Brownian and thermophoresis effects. The effect of the presence of nanoparticles on the convective heat transfer was investigated for different temperature boundary conditions [24], and different geometries including shallow and slender porous cavities [26], and triangular porous cavity [27].

All of the mentioned studies in the literature for convective heat transfer of nanofluids in an enclosure filled with a porous medium have assumed local thermal equilibrium among the phases. The present study aims to examine the free convective heat transfer of nanofluids in a triangular enclosure by using the local thermal non-equilibrium model incorporating Buongiorno's mathematical model [25]. The present study is an extension of the study of Sun and Pop [20] and Sheremet and Pop [27] for the case of local thermal non-equilibrium heat transfer of nanofluids.

Fig. 1. Physical model and coordinate system. [Colour online.]

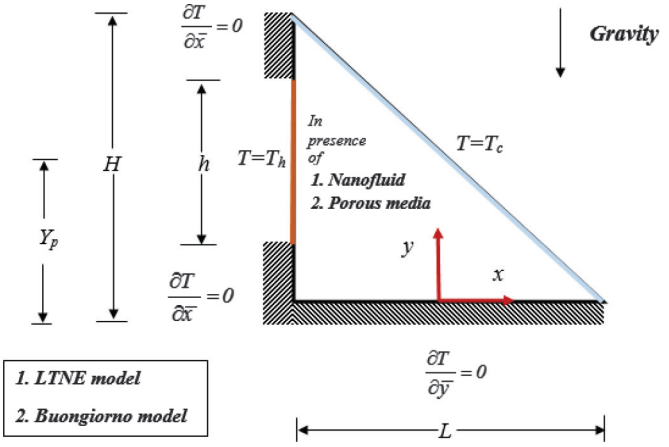

2. Basic equations

Consider the steady state natural convection heat and mass transfer of nanofluids in a two-dimensional porous triangular cavity. The Cartesian coordinate system of $\bar{x}$ and $\bar{y}$ is adopted where the $\bar{x}$ axis is aligned along the bottom wall, and the $\bar{y}$ axis is aligned along the vertical wall. A schematic view of the coordinate system and problem modeling is depicted in Fig. 1.

The height of the vertical wall of the triangle is H while the length of the bottom horizontal wall is L. A heater with height H_H and center position Y_p is mounted at the left vertical wall. The heater holds the temperature of the wall at a constant T_h while the remaining parts of the vertical wall are well insulated. The bottom wall is also well insulated while there are no heat or particles fluxes at the surface. The hypotenuse wall is cooled and maintained at the constant temperature T_c. The flow in the porous medium is modeled using the Darcy–Boussinesq model. The local thermal non-equilibrium model is also employed to account for the temperature difference between the phases. In the heat equations, the temperature difference between the base fluid and nanoparticles as well as the temperature difference between the base fluid and the solid–matrix is taken into account. Therefore, the thermal equations are described by a three-temperature model. It is assumed that the nanoparticles are well suspended in the nanofluid by using either surfactant or surface charge technology that prevents the nanoparticles from agglomeration and deposition on the porous matrix [28–31].

The conservation equations for the total mass of the mixture, Darcy momentum for the mixture, thermal energy in the fluid phase, thermal energy in the particle phase, thermal energy in the solid–matrix phase, and mass of nanoparticles are written as,

$$\nabla \cdot \boldsymbol{V} = 0 \tag{1}$$

$$\frac{\mu}{K}\boldsymbol{V} = -\nabla p + \{C\rho_p + (1-C)\rho_{f0}[1-\beta(T_f - T_c)]\}\boldsymbol{g} \tag{2}$$

$$\frac{1}{\varepsilon}\boldsymbol{V}\cdot\nabla T_f = \frac{k_f}{(\rho c)_f}\nabla^2 T_f + \tau\left(D_B \nabla C\cdot\nabla T_f + \frac{D_T}{T_c}\nabla T_f\cdot\nabla T_f\right) + \frac{h_{fp}(T_p - T_f) + h_{fs}(T_s - T_f)}{\varepsilon(1-C_0)(\rho c)_f} \tag{3}$$

$$\frac{1}{\varepsilon}\boldsymbol{V}\cdot\nabla T_p = \frac{k_p}{(\rho c)_p}\nabla^2 T_p + \frac{h_{fp}}{\varepsilon C_0 (\rho c)_p}(T_f - T_p) \tag{4}$$

$$0 = \frac{k_s}{(\rho c)_s}\nabla^2 T_s + \frac{h_{fs}}{(1-\varepsilon)(\rho c)_s}(T_f - T_s) \tag{5}$$

$$\frac{1}{\varepsilon}\boldsymbol{V}\cdot\nabla C = D_B\nabla^2 C + \frac{D_T}{T_c}\nabla^2 T_f \tag{6}$$

where a detailed derivation of these equations was proposed and discussed by Buongiorno [25], Tzou [32, 33], Nield and Kuznetsov [30], and Kuznetsov and Nield [28]. In the governing equations for the conservation of thermal energy in the fluid phase, (3), as well as the mass conservation for nanoparticles, (6), the Brownian transport and thermophoresis coefficients are assumed to be constant [28, 30] as the temperature differences in the system are assumed to be small. Now, by introducing a stream function $\bar{\psi}$ defined by

$$\bar{u} = \frac{\partial\bar{\psi}}{\partial\bar{y}} \qquad \bar{v} = -\frac{\partial\bar{\psi}}{\partial\bar{x}} \tag{7}$$

the continuity equation for the mixture, (1), is satisfied identically. The pressure could also be eliminated from the momentum equation, (2), by cross differentiation. Hence, the remaining equations can be written as,

$$\frac{\partial^2\bar{\psi}}{\partial\bar{x}^2} + \frac{\partial^2\bar{\psi}}{\partial\bar{y}^2} = -\frac{(1-C_0)\rho_{f0}gK\beta}{\mu}\frac{\partial T_f}{\partial\bar{x}} + \frac{\rho_p - \rho_{f0}}{\mu}gK\frac{\partial C}{\partial\bar{x}} \tag{8}$$

$$\begin{aligned}\frac{1}{\varepsilon}\left(\frac{\partial\bar{\psi}}{\partial\bar{y}}\frac{\partial T_f}{\partial\bar{x}} - \frac{\partial\bar{\psi}}{\partial\bar{x}}\frac{\partial T_f}{\partial\bar{y}}\right) &= \alpha_f\left(\frac{\partial^2 T_f}{\partial\bar{x}^2} + \frac{\partial^2 T_f}{\partial\bar{y}^2}\right)\\ &+ \tau\left\{D_B\left(\frac{\partial C}{\partial\bar{x}}\frac{\partial T_f}{\partial\bar{x}} + \frac{\partial C}{\partial\bar{y}}\frac{\partial T_f}{\partial\bar{y}}\right) + \left(\frac{D_T}{T_c}\right)\left[\left(\frac{\partial T_f}{\partial\bar{x}}\right)^2 + \left(\frac{\partial T_f}{\partial\bar{y}}\right)^2\right]\right\}\\ &+ \frac{h_{fp}(T_p - T_f) + h_{fs}(T_s - T_f)}{\varepsilon(1-C_0)(\rho c)_f}\end{aligned} \tag{9}$$

$$\frac{1}{\varepsilon}\left(\frac{\partial\bar{\psi}}{\partial\bar{y}}\frac{\partial T_p}{\partial\bar{x}} - \frac{\partial\bar{\psi}}{\partial\bar{x}}\frac{\partial T_p}{\partial\bar{y}}\right) = \alpha_p\left(\frac{\partial^2 T_p}{\partial\bar{x}^2} + \frac{\partial^2 T_p}{\partial\bar{y}^2}\right) + \frac{h_{fp}}{\varepsilon C_0(\rho c)_p}(T_f - T_p) \tag{10}$$

$$0 = \alpha_s\left(\frac{\partial^2 T_s}{\partial\bar{x}^2} + \frac{\partial^2 T_s}{\partial\bar{y}^2}\right) + \frac{h_{fs}}{(1-\varepsilon)(\rho c)_s}(T_f - T_s) \tag{11}$$

$$\frac{1}{\varepsilon}\left(\frac{\partial\bar{\psi}}{\partial\bar{y}}\frac{\partial C}{\partial\bar{x}} - \frac{\partial\bar{\psi}}{\partial\bar{x}}\frac{\partial C}{\partial\bar{y}}\right) = D_B\left(\frac{\partial^2 C}{\partial\bar{x}^2} + \frac{\partial^2 C}{\partial\bar{y}^2}\right) + \left(\frac{D_T}{T_c}\right)\left(\frac{\partial^2 T_f}{\partial\bar{x}^2} + \frac{\partial^2 T_f}{\partial\bar{y}^2}\right) \tag{12}$$

where these governing equations can be represented in the non-dimensional form by invoking the following non-dimensional variables:

$$\begin{aligned}&x = \frac{\bar{x}}{L} \qquad y = \frac{\bar{y}}{L} \qquad \psi = \frac{\bar{\psi}}{\alpha_f} \qquad \phi = \frac{C}{C_0}\\ &\theta_f = \frac{T_f - T_c}{T_h - T_c} \qquad \theta_p = \frac{T_p - T_c}{T_h - T_c} \qquad \theta_s = \frac{T_s - T_c}{T_h - T_c}\end{aligned} \tag{13}$$

as,

$$\frac{\partial^2\psi}{\partial x^2} + \frac{\partial^2\psi}{\partial y^2} = -\mathrm{Ra}\frac{\partial\theta_f}{\partial x} + \mathrm{RaNr}\frac{\partial\phi}{\partial x} \tag{14}$$

$$\begin{aligned}\frac{\partial\psi}{\partial y}\frac{\partial\theta_f}{\partial x} - \frac{\partial\psi}{\partial x}\frac{\partial\theta_f}{\partial y} &= \varepsilon\left(\frac{\partial^2\theta_f}{\partial x^2} + \frac{\partial^2\theta_f}{\partial y^2}\right) + \mathrm{Nb}\left(\frac{\partial\phi}{\partial x}\frac{\partial\theta_f}{\partial x} + \frac{\partial\phi}{\partial y}\frac{\partial\theta_f}{\partial y}\right)\\ &+ \mathrm{Nt}\left[\left(\frac{\partial\theta_f}{\partial x}\right)^2 + \left(\frac{\partial\theta_f}{\partial y}\right)^2\right] + \mathrm{Nhp}(\theta_p - \theta_f) + \mathrm{Nhs}(\theta_s - \theta_f)\end{aligned} \tag{15}$$

$$\frac{\partial\psi}{\partial y}\frac{\partial\theta_p}{\partial x} - \frac{\partial\psi}{\partial x}\frac{\partial\theta_p}{\partial y} = \varepsilon_p\left(\frac{\partial^2\theta_p}{\partial x^2} + \frac{\partial^2\theta_p}{\partial y^2}\right) + \mathrm{Nhp}\gamma_p(\theta_f - \theta_p) \tag{16}$$

$$0 = \frac{\partial^2\theta_s}{\partial x^2} + \frac{\partial^2\theta_s}{\partial y^2} + \mathrm{Nhs}\gamma_s(\theta_f - \theta_s) \tag{17}$$

$$\frac{\partial\psi}{\partial y}\frac{\partial\phi}{\partial x} - \frac{\partial\psi}{\partial x}\frac{\partial\phi}{\partial y} = \frac{1}{\mathrm{Le}}\left(\frac{\partial^2\phi}{\partial x^2} + \frac{\partial^2\phi}{\partial y^2}\right) + \frac{\mathrm{Nt}}{\mathrm{LeNb}}\left(\frac{\partial^2\theta_f}{\partial x^2} + \frac{\partial^2\theta_f}{\partial y^2}\right) \tag{18}$$

By using the non-dimensional parameters, the length and position of the heater and the aspect ratio of the triangle can be represented in non-dimensional form as,

$$Y_p = \frac{y_p}{H} \qquad H_H = \frac{h}{H} \qquad \mathrm{AR} = \frac{L}{H} \tag{19}$$

By considering the problem description and the schematic view of the model in Fig. 1, the boundary conditions for the problem in non-dimensional form are given by,

$$\begin{aligned}&\psi\left(-\frac{\mathrm{AR}}{2}, 1 - H_H\right) = 0\\ &\left.\frac{\partial\theta_f}{\partial x}\right|_{\left(-\frac{AR}{2},1-H_H\right)} = \left.\frac{\partial\theta_p}{\partial x}\right|_{\left(-\frac{AR}{2},1-H_H\right)} = \left.\frac{\partial\theta_s}{\partial x}\right|_{\left(-\frac{AR}{2},1-H_H\right)} = 0\\ &\left.\frac{\partial\phi}{\partial x}\right|_{\left(-\frac{AR}{2},1-H_H\right)} = 0\end{aligned} \tag{20}$$

$$\begin{aligned}&\psi\left(-\frac{\mathrm{AR}}{2}, H_H\right) = 0\\ &\theta_f\left(-\frac{\mathrm{AR}}{2}, H_H\right) = \theta_p\left(-\frac{\mathrm{AR}}{2}, H_H\right) = \theta_s\left(-\frac{\mathrm{AR}}{2}, H_H\right) = 1\\ &\mathrm{Nb}\left.\frac{\partial\phi}{\partial x}\right|_{\left(-\frac{AR}{2},H_H\right)} + \mathrm{Nt}\left.\frac{\partial\theta}{\partial x}\right|_{\left(-\frac{AR}{2},H_H\right)} = 0\end{aligned} \tag{21}$$

$$\psi(x,0) = 0 \qquad \left.\frac{\partial\theta_f}{\partial y}\right|_{(x,0)} = \left.\frac{\partial\theta_p}{\partial y}\right|_{(x,0)} = \left.\frac{\partial\theta_s}{\partial y}\right|_{(x,0)} = 0 \qquad \left.\frac{\partial\phi}{\partial y}\right|_{(x,0)} = 0 \tag{22}$$

$$\begin{aligned}&\psi\left(x, -\frac{x}{\mathrm{AR}} + \frac{1}{2}\right) = 0\\ &\theta_f\left(x, -\frac{x}{\mathrm{AR}} + \frac{1}{2}\right) = \theta_p\left(x, -\frac{x}{\mathrm{AR}} + \frac{1}{2}\right) = \theta_s\left(x, -\frac{x}{\mathrm{AR}} + \frac{1}{2}\right) = 0\\ &\mathrm{Nb}\left.\frac{\partial\phi}{\partial n}\right|_{\left(x,-\frac{x}{AR}+\frac{1}{2}\right)} + \mathrm{Nt}\left.\frac{\partial\theta}{\partial n}\right|_{\left(x,-\frac{x}{AR}+\frac{1}{2}\right)} = 0 \quad \text{for} \quad -\frac{\mathrm{AR}}{2} \le x \le +\frac{\mathrm{AR}}{2}\end{aligned} \tag{23}$$

where Nb, Nt, Nr and Le denote the Brownian motion parameter, thermophoresis parameter, buoyancy ratio parameter, and Lewis number, respectively. The Nhp and Nhs show the interface heat transfer parameters for the nanoparticle base fluid and the porous matrix – base fluid, known as Nield numbers [34]. Finally, ε_p, γ_p, and γ_s, depict a modified thermal diffusivity ratio for nanoparticles, modified thermal capacity ratio for nanoparticles, and modified thermal conductivity ratio for the porous phase. These parameters are defined as,

$$\mathrm{Nr}=\frac{(\rho_p-\rho_{f0})C_0}{\rho_{f0}\beta\Delta T(1-C_0)} \quad \mathrm{Nb}=\frac{\tau D_B C_0 \varepsilon}{\alpha_f} \quad \mathrm{Nt}=\frac{\tau D_T \varepsilon \Delta T}{\alpha_f T_c}$$
$$\mathrm{Nhp}=\frac{h_{fp}L^2}{k_f(1-C_0)} \quad \mathrm{Nhs}=\frac{h_{fs}L^2}{k_f(1-C_0)} \quad \varepsilon_p=\frac{\alpha_p \varepsilon}{\alpha_f} \tag{24}$$
$$\gamma_p=\frac{(1-C_0)(\rho c)_f}{C_0(\rho c)_p} \quad \gamma_s=\frac{k_f(1-C_0)}{k_s(1-\varepsilon)} \quad \mathrm{Le}=\frac{\alpha_f}{D_B\varepsilon}$$

Here, the physical quantities of interest are the local and average heat and mass transfer from the left vertical wall. The local Nusselt numbers for the base fluid, nanoparticles and the solid matrix (i.e., $\mathrm{Nu_f}$, $\mathrm{Nu_p}$, $\mathrm{Nu_s}$) and the local Sherwood number Sh for nanoparticles are defined as,

$$\mathrm{Nu_f}=-\left(\frac{\partial\theta_f}{\partial x}\right)_{x=-\frac{AR}{2}} \quad \mathrm{Nu_p}=-\left(\frac{\partial\theta_p}{\partial x}\right)_{x=-\frac{AR}{2}}$$
$$\mathrm{Nu_s}=-\left(\frac{\partial\theta_s}{\partial x}\right)_{x=-\frac{AR}{2}} \quad \mathrm{Sh}=-\left(\frac{\partial\phi}{\partial x}\right)_{x=-\frac{AR}{2}} \tag{25}$$

The average Nusselt and Sherwood numbers for the left wall are defined as,

$$\overline{\mathrm{Nu_f}}=\int_0^1 \mathrm{Nu_f}dy \quad \overline{\mathrm{Nu_p}}=\int_0^1 \mathrm{Nu_p}dy$$
$$\overline{\mathrm{Nu_s}}=\int_0^1 \mathrm{Nu_s}dy \quad \overline{\mathrm{Sh}}=\int_0^1 \mathrm{Sh}dy \tag{26}$$

It is worth mentioning that Sherwood number is a function of temperature gradient of the fluid phase due to the adopted boundary condition for surface impermeability to nanoparticles (i.e., (23) as $\partial\phi/\partial x=-(\mathrm{Nt}/\mathrm{Nb})(\partial\theta_f/\partial x)$). Thus, the analysis of the local and average Sherwood number is easily possible through analysis of Nusselt number for the fluid phase. Therefore, the local and average Sherwood number are written as $\mathrm{Sh}=(\mathrm{Nt}/\mathrm{Nb})\mathrm{Nu_f}$ and $\overline{\mathrm{Sh}}=(\mathrm{Nt}/\mathrm{Nb})\overline{\mathrm{Nu_f}}$, and hence, the results will be strictly reported for Nusselt number.

3. Numerical method and validation

The set of partial differential equations, (14)–(18), and the corresponding boundary conditions at the walls (i.e., (23)) are solved by employing the finite element method [35, 36]. In this regard, the governing equations were formulated in the weak form [35, 36]. In the finite element method, the quadratic elements and the Lagrange shape function were utilized [35]. The governing equations for momentum, thermal energy of phases, and the conservation of nanoparticles were fully coupled using the damped Newton method [36]. A parallel sparse direct solver [37] was employed to solve the corresponding algebraic equations. The computations were continued until the residuals for the each of the residual equations became smaller than 10^{-6}. The solution procedure, in the form of an in-house computational fluid dynamics code, has been validated successfully against the works of Sun and Pop [20], Baytas and Pop [38], Chamkha and Ismael [7], Chamkha et al. [39], and Costa [40] for natural convection in porous media in enclosures. More details regarding the utilized finite element solution procedure can be found in excellent references by Gross and Reusken [41] and Wriggers [36].

Review of previous studies indicates that the magnitude of Brownian motion (Nb) and thermophoresis (Nt) parameters are very small, on the order of 10^{-6} [42, 43]. The buoyancy ratio parameter (Nr) is higher than unity, and the Lewis number is very large, on the order of 10^3 and higher because of the very low magnitude of the Brownian defensive coefficient in nanofluids [44, 45]. The interface heat transfer parameters for the nanoparticle – base fluid and porous matrix – base fluid, Nield numbers (Nhp and Nhs), are higher than unity [46]. The modified thermal capacity ratio for nanoparticles (γ_p) and the modified thermal conductivity ratio for porous phase (γ_s) are on the order of 10. Finally, the modified thermal diffusivity ratio (ε_p) is of order one. The geometric parameters Y_p and H_H can be varied about the range of 0 to 1, and the aspect ratio is considered in the range of 0.1 to 10. Finally, the Darcy–Rayleigh number is considered on the order of 100. Here, according to the discussed range of non-dimensional parameters, in the present study the results are reported for Ra = 100, Nb = 10^{-6}, Nt = 10^{-6}, Le = 1000, Nr = 5.0, Nhs = 10.0, Nhp = 10.0, γ_s = 10.0, γ_p = 10.0 ε = 0.5, ε_p = 1.0, Y_p = 0.7, Ht = 0.5, and AR = 1.0 and otherwise the value of the parameter will be stated. Table 1 shows the average Nusselt numbers of various phases for the mentioned typical case for different grid sizes. The results are reported for two interface heat transfer parameters of low interface heat interaction of Nhp = Nhs = 10 and high interface thermal interaction of Nhp = Nhs = 20. As seen in Table 1, the grid size of 100 × 100 provides adequate accuracy for most engineering applications and graphical representation of the results. Hence, the results of figures are obtained with a mesh consisting of 100 × 100 grid points.

The results of the present study are compared with the classical benchmark study of heat transfer of a pure fluid in a differentially heated square cavity by neglecting the Brownian motion and thermophoresis effects and assuming local thermal equilibrium between phases. The average Nusselt number results are shown in Table 2. As seen, in this case there is a very good agreement with the previous studies available in the literature.

Sun and Pop [20] studied the convective heat transfer of nanofluids in a triangular enclosure filled with a nanofluid-saturated porous medium. The researchers neglected Brownian motion and thermophoresis effects and utilized a single-phase model for nanofluids. They have also assumed local thermal equilibrium among all three phases of the nanoparticles, the base fluid, and the porous matrix. Hence, by neglecting the Brownian motion and thermophoresis effects (Nb = Nt = 0), and also by neglecting the temperature difference between phases, the present study reduces to the study of Sun and Pop [20]. In this case, a comparison between the results of present study and those reported by Sun and Pop [20] is performed in Fig. 2 for AR = 1 and H_H = 0.4 as well as H_H = 0.8. In Fig. 2 the results are reported for different values of Rayleigh number. This figure shows excellent agreement with the results available in the literature.

Shermet and Pop [27] studied the free convective heat transfer of nanofluids in a triangular cavity filled with porous medium when the total of the vertical wall is at constant temperature T_h. The authors adopted the constant concentration of C_c and C_h for nanoparticles at the cold and hot walls and assumed local thermal equilibrium between phases. By considering the form of the obtained governing equations and boundary conditions in the study of Shermet and Pop [27], the results of the present study are compared with those of the previous research in Fig. 3 for local Nusselt number at the vertical wall. Figure 3 shows good agreement between the present results and those reported by Shermet and Pop [27].

4. Results and discussion

Figure 4 shows the effect of buoyancy ratio parameter (Nr) on the streamlines in a triangular cavity. In this figure, the streamlines are plotted for two values of Nr = 0 and 10. This figure clearly shows the clockwise circulation of the nanofluid inside the enclosure. The nanofluid next to the hot wall absorbs the thermal energy and gets hot. The hot nanofluid is lighter than the cold one and as a result it moves in the upward direction. Then the hot flow

Table 1. Grid independency test for Ra = 100, Nb = 10^{-6}, Nt = 10^{-6}, Le = 1000, Nr = 5.0, γ_s = 10.0, γ_p = 10.0 ε = 0.5, ε_p = 1.0, Y_p = 0.5, Ht = 0.7, and AR = 1.0.

	Nhp = Nhs = 10			Nhp = Nhs = 20		
Grid size	Nu_f	Nu_s	Nu_p	Nu_f	Nu_s	Nu_p
50×50	5.27	3.72	4.25	5.22	3.89	4.38
100×100	5.34	3.73	4.28	5.30	3.90	4.41
150×150	5.37	3.74	4.29	5.32	3.90	4.43
200×200	5.37	3.74	4.30	5.32	3.91	4.43

Table 2. Average Nusselt number of the hot wall.

	Nu	
Source	Ra = 100	Ra = 1000
[1]	3.16	14.06
[47]	3.11	—
[48]	3.14	13.45
[49]	3.12	13.64
[50]	2.80	—
[51]	4.2	15.8
[52]	3.097	12.96
Present results	3.11	13.64

Fig. 2. Evaluated average Nusselt number with the results of Sun and Pop [20]. [Colour online.]

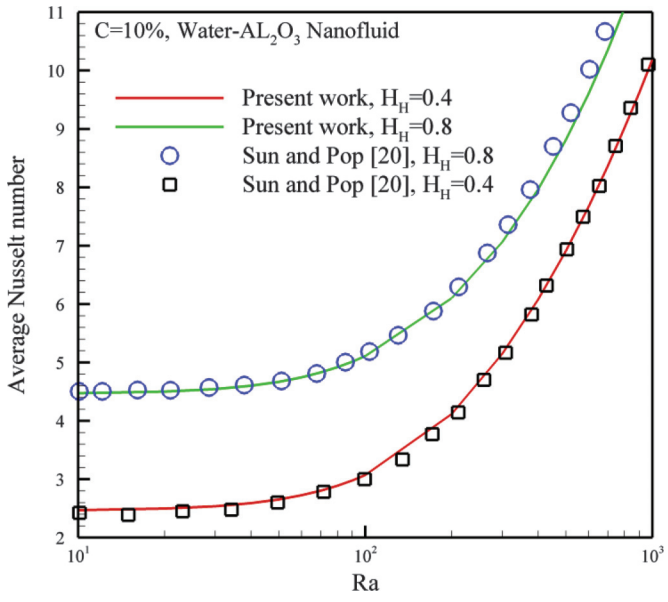

Fig. 3. Local Nusselt number of the present work and Sheremet and Pop [27] when Nr = Nb = Nt = 0.1. [Colour online.]

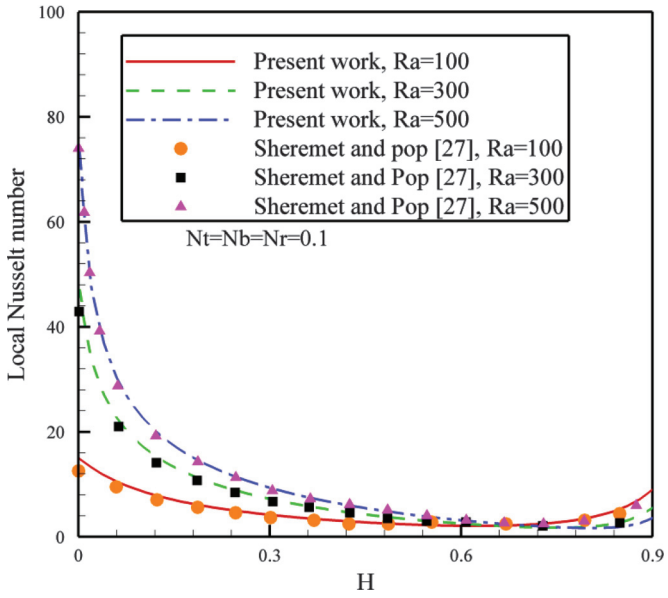

Fig. 4. Streamlines of nanofluid in Nr = 0 (black line) and Nr = 10 (red line). [Colour online.]

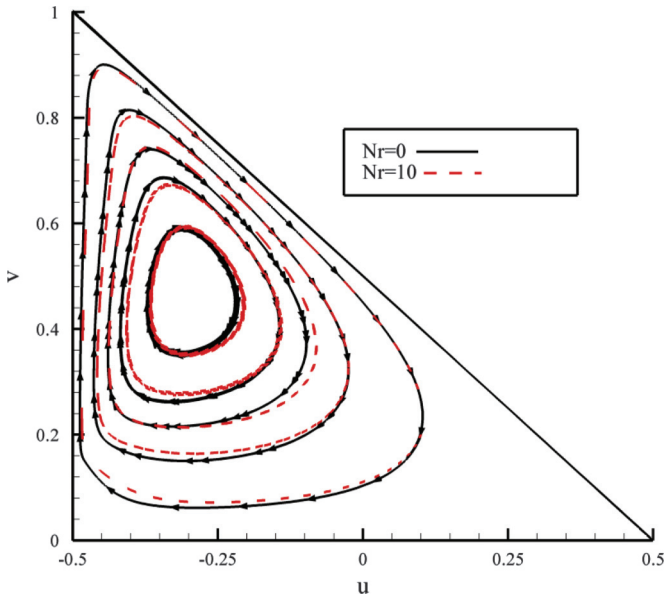

reaches the cold inclined wall, in which the nanofluid loses a part of its thermal energy and flows in a downward direction.

Figure 4 shows that the presence of buoyancy effects due to mass transfer of nanoparticles induces a significant effect on the streamlines. Indeed, the thermophoresis force tends to move the nanoparticles away from the hot heater and push them into the cold inclined wall. It is clear that the migration of the heavy nanoparticles from one region to another region results in the buoyancy forces that consequently affect the streamlines.

Figure 5 compares the non-dimensional temperature distribution of the three phases of nanoparticles (θ_p), the base fluid (θ_f), and the solid porous matrix (θ_s) in the enclosure. This figure indicates that near the top corner of the cavity, the temperature differences among the phases are small. In this region, the temperature profiles are very close together, and hence, the corresponding temperature gradients are strong. In contrast, at the right and the bottom areas of the triangular enclosure, the levels of temperature profiles are not very close together, and hence, the temperature gradients are also low. Figure 5 illustrates the temperature profiles for each phase. The differences between the temperatures of the different phases are more obvious in the right and bottom of the enclosure where the flow velocities are small. The temperature distribution of the base fluid next to the heater is under the significant effect of fluid flow and shows a boundary layer shape. However, the temperature distribution in the solid

Fig. 5. Isothermal contours of fluid (green line, θ_f), solid (red dashed line, θ_s), and nanoparticles (blue long dashed, θ_p). [Colour online.]

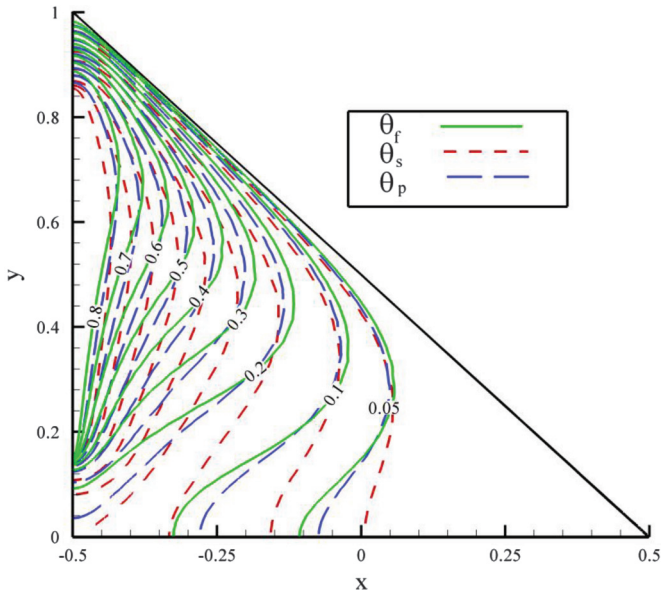

Fig. 6. Concentration of nanoparticles in triangular cavity. [Colour online.]

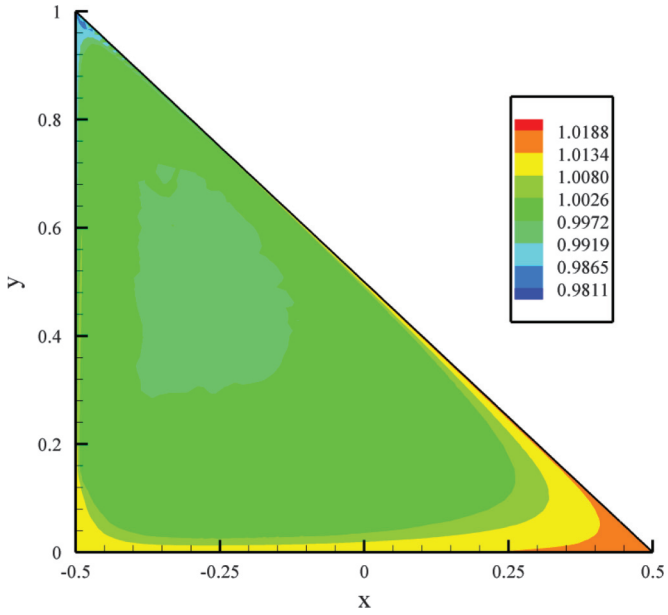

matrix shows a distribution almost similar to the pure conduction in solids, but variation because of the effect of the thermal interaction between the base fluid and nanoparticles is also obvious in the temperature distribution of this phase. The temperature distribution of nanoparticles almost follows the temperature distribution of the base fluid, but they are not identical as the interaction parameter (Nhp) between nanoparticles and base fluid phase is assumed to be finite.

Figure 6 shows the concentration distribution of nanoparticles in the triangular cavity. As seen, the concentration of nanoparticles in the vicinity of the heater is low, and in contrast, it is high in the vicinity of the inclined cold wall. This distribution of concentration of nanoparticles is due to the thermophoresis forces, which tend to move the nanoparticles from the hot wall toward the cold one. In addition, Fig. 6 clearly shows that the concentration gradients of nanoparticles near the walls is high, but the concentration of nanoparticles in the core region of the enclosure is almost uniform. The high concentration gradients next to the hot and cold walls are due to the high values of Lewis number. Indeed, the Brownian coefficient for diffusion of nanoparticles is very low, and hence, the concentration gradient of nanoparticles is very high.

Figures 7 shows the effect of interface heat parameters for nanoparticles (i.e., Nhp) on the temperature distribution in the nanoparticle phase. The isotherms for the base fluid when Nhp = 10 (the typical case) are also plotted in this figure for the sake of comparison. Figure 7 shows that the increase of the heat transfer parameter for nanoparticles tends to shift the nanoparticle phase isotherms toward the cold wall. Indeed, the increase of the interface parameter (i.e., Nhp) indicates a higher thermal interaction between the nanoparticles and the base fluid phases. Because of the increase of the interaction between nanoparticles and the base fluid, the nanoparticles tend to follow the temperature profiles of the base fluid phase. It is also interesting that the most dominant effect of the variation of Nhp occurrs next to the bottom adiabatic wall. This is where the flow is slow and the interaction between the fluid phase and the nanoparticles plays a significant role.

Figure 8 shows the effect of the interface heat parameter for the porous phase (i.e., Nhs) on the temperature distribution in the porous matrix phase. In this figure, the isotherms of the fluid

Fig. 7. Isothermal contours of nanoparticles in Nhp = 5 (red dashed line), Nhp = 10 (black line). [Colour online.]

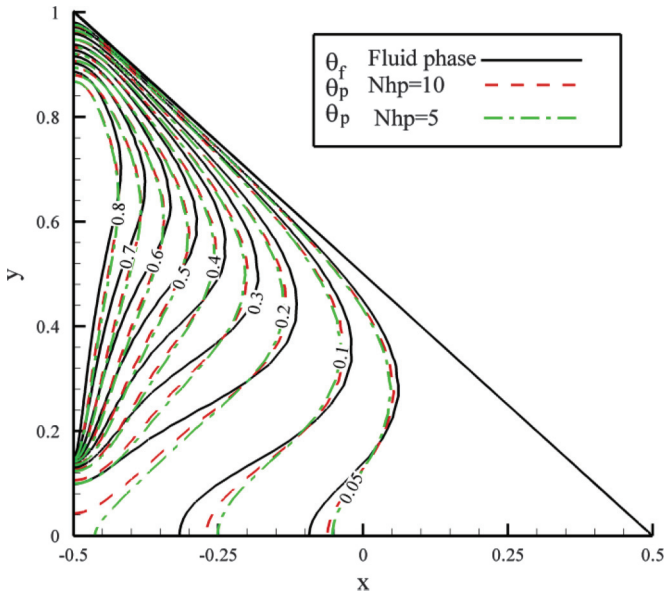

phase for the default set of non-dimensional parameters are also plotted for the sake of comparison. This figure shows that the increase of the interface interaction between the base fluid phase and the porous medium phase tends to shift the isotherms into the base fluid temperature.

The most significant temperature differences between the base fluid phase and the porous medium phase are in bottom of the enclosure where the nanofluid velocity is slow. The same trends of behaviors were also observed for the nanoparticles in Fig. 7, but here the difference between the isotherms is more distinct. This is because the tiny nanoparticles would more easily follow the base fluid behavior rather than the solid porous matrix.

Fig. 8. Isothermal contours of solid (porous media) for Nhs = 5 (red dashed line) and Nhs = 10 (black solid line). [Colour online.]

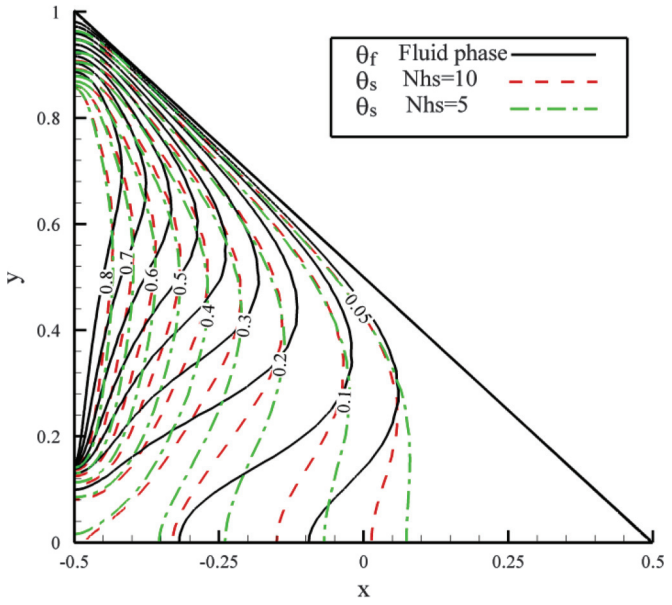

Fig. 9. Local Nusselt number of fluid phase (Nu_f), solid phase (Nu_s) and nanofluid (Nu_p) on heater in size of $H_H = 0.7$. [Colour online.]

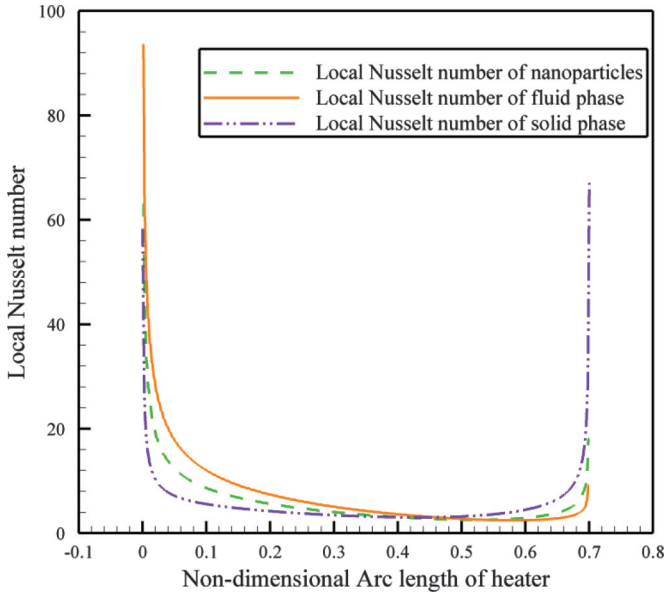

Figure 9 compares the profiles of local Nusselt number of porous medium, base fluid, and nanoparticle phases evaluated on the flush-mounted heater at the vertical wall. The *x* axis in this figure is the arc length of the heater measured from the bottom of the heater. At the bottom of the heater where the fluid began to be heated, the local Nusselt number is significantly higher. This is because the fresh-cooled nanofluid starts to absorb heat from the heater, and hence, the heat transfer rate due to the diffusion mechanism is high. Then, the local Nusselt number falls rapidly to a fixed low level of average Nusselt number. This is where the temperature of the porous matrix, nanoparticles, and the base fluid next to the wall starts raising. The increase in the temperature next to the wall reduces the temperature difference between the wall and its surrounding, which results in a decrease of the heat transfer. In this region, the heat would be removed by both the diffusive and advective mechanisms, simultaneously. Finally, a sudden increase in local Nusselt number can be observed at the top of the heater. This region is connected to the unheated surrounding areas, tending to strongly absorb heat from the heater element. This figure also shows that the local Nusselt number for the base fluid is very high at the bottom of the heater, but is very low at the top of the heater. Indeed, when the fresh cold water reaches the heater element, it tends to strongly absorb the heat from the heater element. In this case, the nanofluid not only carries the absorbed heat but also passes it into the surrounding medium. In contrast, the nanofluid's temperature increases as it passes over the heater, and hence, the local Nusselt number reduces along the heater length moving from bottom to top. Next to the end of the heater, the liquid is under the smoothing effect of the unheated surrounding media. However, it should be noted that the flow is in the upward direction. Thus, the effect of low temperature surroundings cannot be well passed through the fluid stream into the heater.

The porous matrix phase shows comparatively high values of local Nusselt number at the bottom and top parts of the heater. This is because the heat transfer in porous matrix is dominant by the diffusion mechanism. Hence, at the top of the heater, the porous matrix can absorb the heat from the heater as well as the bottom of the heater. The smooth difference between the local Nusselt number for the porous phase at the bottom and the top of the heater is the result of the interaction between this phase and the base fluid phase.

Figure 10 compares the profiles of local Nusselt number for selected combinations of the interface heat parameters. As seen, the increase of Nhp tends to smoothly shift the behavior of the local Nusselt profiles of the nanoparticle phase towards the behavior of the base fluid phase (which was depicted in Fig. 9). Like the nanoparticle phase, the increase of Nhs tends to shift the behaviour of the local Nusselt number of the porous phase towards that of the base fluid phase, which was seen in Fig. 9.

Table 3 shows the effect of the enclosure size on the average Nusselt number of the studied phases. Figures 11 and 12 show the corresponding streamlines and isotherms for a triangular enclosure of AR = 0.5 and 2.0. It is worth mentioning that the corresponding streamlines and isotherms for AR = 1 were depicted in Figs. 4 and 5. It is clear that the increase of the aspect ratio decreases the heat transfer in the enclosure. Increasing aspect ratio results in a wider dead area in the bottom of the enclosure. Indeed, when the aspect ratio decreases, the hot and cold walls are get closer, and hence, the Nusselt number increases.

Figures 13–15 show the effect of interface parameters (i.e., Nhs and Nhp) on the average Nusselt numbers of the fluid phase, the nanoparticle phase, and the porous medium phase, respectively. Figure 13 shows that the increase of the interface parameters (i.e., Nhs and Nhp) reduces the heat transfer of the fluid phase at the vertical wall (the raise of Nu_f). In fact, the increase of the interface heat transfer parameters increases the interaction between the phases and reduces the temperature difference between the wall and the fluid in the vicinity of the wall, which ultimately results in a lower rate of the heat transfer through the base fluid phase.

Figure 14 reveals that the addition of the interface heat transfer parameter for nanoparticles, Nhp, would significantly raise the average Nusselt number for the nanoparticle phase. In Fig. 13, it was found that Nu_f is a decreasing function of Nhp, which shows that the interaction between the nanoparticles and fluid phase tends to reduce the temperature difference between the fluid phase and the hot wall. The decrease of the temperature difference between the hot wall and the base fluid phase means that the temperature of the base fluid next to the wall is increased by the interaction with nanoparticles. This is only possible when the temperature of the fluid phase is lower than the temperature of

Fig. 10. Local Nusselt number of solid phase and nanoparticles on heater in size of H_H = 0.7. [Colour online.]

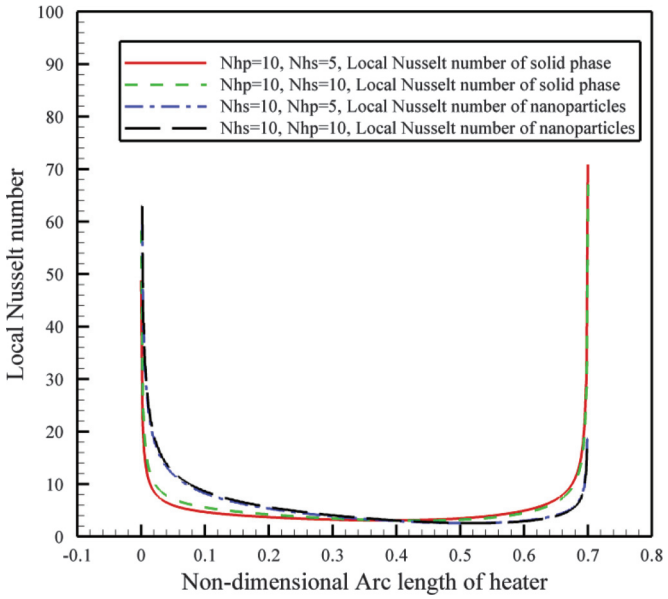

Table 3. Evaluation of average Nusselt number of fluid phase ($\overline{Nu}_s$), solid phase ($\overline{Nu}_p$), and nanofluid in several aspect ratios.

AR	$\overline{Nu}_f$	$\overline{Nu}_s$	$\overline{Nu}_p$
0.5	5.72	4.46	5.19
1	4.60	2.88	3.95
2	3.94	2.23	3.38

the nanoparticles, and in this case, the hot nanoparticles will lose a part of their thermal energy to the fluid phase. When the nanoparticles pass their thermal energy to their surrounding base fluid, their temperature falls down, and consequently, the temperature difference between nanoparticles and the hot wall increases. The increase of the temperature difference between the nanoparticles and the hot wall results in the increase of the heat transfer rate (the increase of $\overline{Nu}_p$), and consequently, the gradient of the nanoparticle temperature phase rises. This outcome can be clearly seen Fig. 14.

Figure 14 shows that the addition of the interface heat transfer parameter for the porous phase, Nhs, smoothly reduces the heat transfer rate in the nanoparticle phase ($\overline{Nu}_p$). The increase of interaction between the porous matrix and the fluid phase tends to increase the temperature of the fluid phase in the vicinity of the hot wall. When the temperature of the base fluid increases because of interaction with the porous matrix, the temperature of the fluid phase could be close to the temperature of the nanoparticles or higher; hence, the fluid phase would absorb a small amount of heat from the nanoparticles or pass some amount of heat to the nanoparticles. The results of Fig. 14 show that for high values of the interaction parameter between the base fluid and porous matrix phases, Nhs = 10, the fluid phase would pass some amount of thermal energy to the nanoparticles, and hence, the temperature of the nanoparticles is increased. The increase of the nanoparticle temperature next to the heater reduces the temperature gradient and consequently reduces the average Nusselt number for the nanoparticle phase.

Fig. 11. (*a*) Isotherm contours of fluid phase (θ_f), solid phase (θ_s) and nanoparticles (θ_p) and (*b*) streamlines (ψ) in AR = 0.5. [Colour online.]

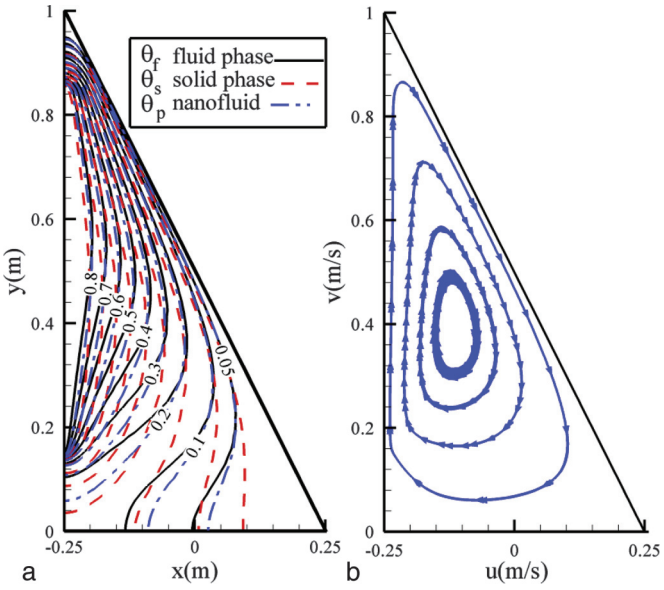

Fig. 12. (*a*) Isotherm contours of fluid phase (θ_f), solid phase (θ_s) and nanoparticles (θ_p) and (*b*) streamlines (ψ) in AR = 2. [Colour online.]

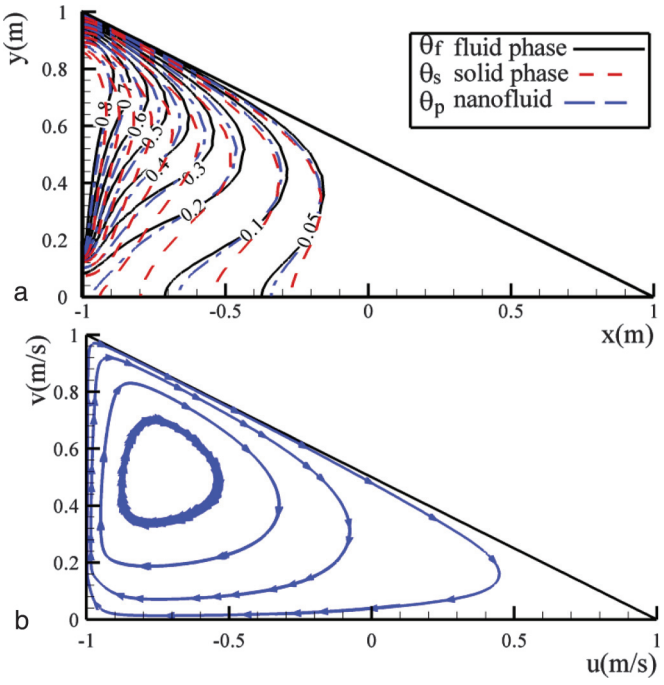

Figure 15 shows the effect of interface heat transfer parameters on the heat transfer rate of the porous medium phase. The augmentation of the interface heat transfer parameter, Nhs, for the porous phase significantly increases the average Nusselt number for this phase. This is because the addition of Nhs increases the thermal interaction between the fluid phase and the porous phase, which results in the increase of the temperature of the fluid phase (the observed decrease of $\overline{Nu}_f$ in Fig. 13) and simultaneously the reduction of the porous phase temperature. The reduction of the temperature of the porous matrix, next to the heater, would consequently increase the average Nusselt number

Fig. 13. Average Nusselt number of fluid ($\overline{Nu}_f$) as a function buoyancy ratio (Nr). [Colour online.]

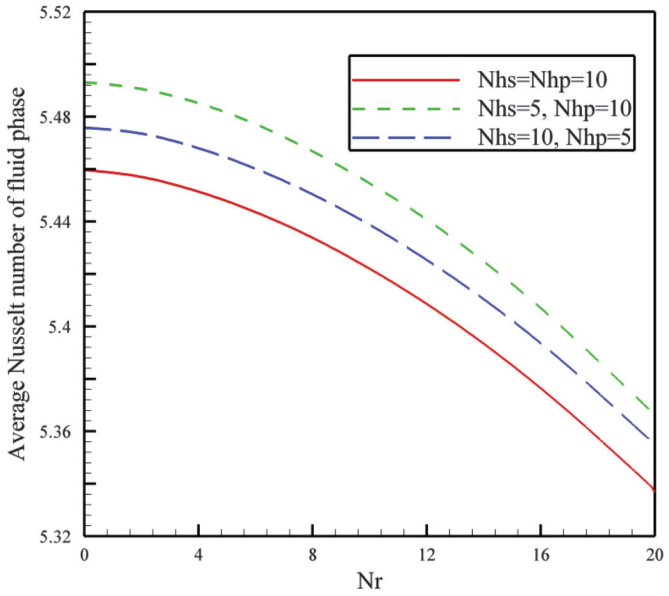

Fig. 14. Average Nusselt number of nanoparticles ($\overline{Nu}_p$) as a function of buoyancy ratio (Nr). [Colour online.]

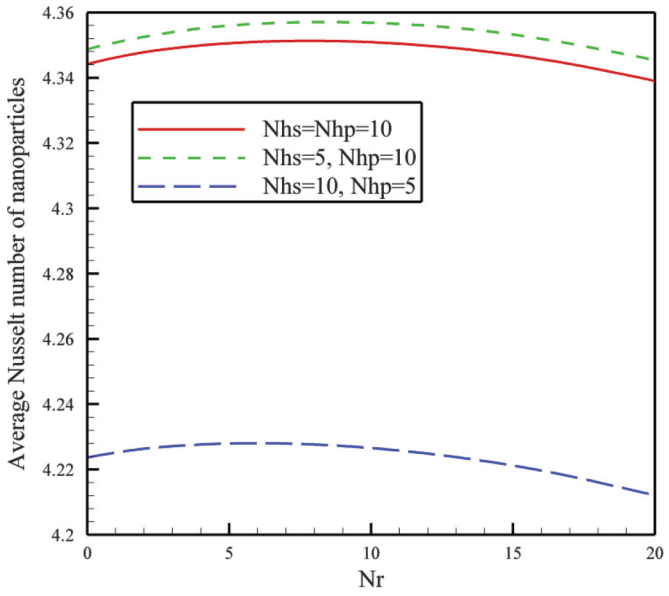

Fig. 15. Average Nusselt number of porous media ($\overline{Nu}_s$) as a function of buoyancy ratio (Nr). [Colour online.]

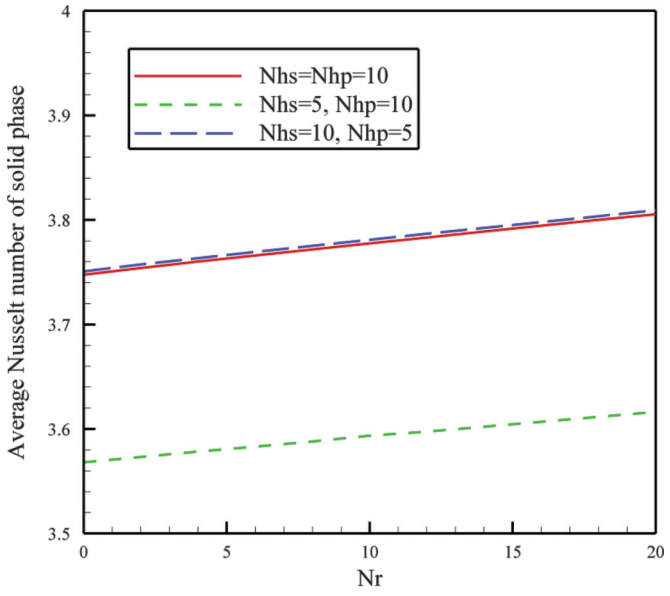

Fig. 16. Average Nusselt number as a function of Rayleigh number. [Colour online.]

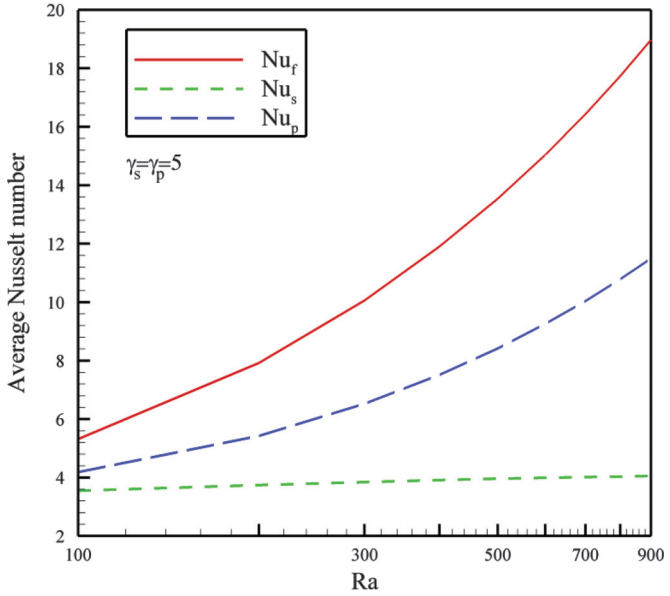

(temperature gradient in the porous phase). Finally, the increase of Nhp would smoothly decrease the average Nusselt number of the porous phase. Indeed, the addition of Nhp increases the heat transfer interaction between the base fluid and nanoparticles, which results in the increase of the fluid phase temperature. When the temperature of the fluid phase rises, the absorbed heat from the porous matrix by the base fluid decreases. Hence, the temperature difference between the wall and the porous matrix remains low, and consequently, the temperature gradient in the porous phase is low.

Figure 16 compares the magnitude of the average Nusselt numbers of different phases against various values of Rayleigh number. This figure interestingly depicts that an increase in the Rayleigh number significantly boosts the average Nusselt number of the base fluid phase and the nanoparticle phase. However, the average Nusselt number for the porous phase is a very smooth increasing function of Rayleigh number. The increase of the Rayleigh number increases the fluid flow and thereby enhances the advective mechanisms, which results in the increase of the Nusselt number for the nanoparticles and the base fluid phases. However, the solid porous medium is stationery and does not directly incorporate into the advective mechanisms. The smooth variation of average Nusselt number of the porous phase is due to the interaction between the porous media and the fluid phase through the interface heat transfer mechanism for the porous phase (Nhs).

Figures 17–19 show the effect of the modified heat capacity for nanoparticles (γ_p) and the modified thermal conductivity for po-

Fig. 17. Average Nusselt number of fluid phase ($\overline{Nu}_f$) as a function of modified thermal capacity ratio of nanoparticles (γ_p). [Colour online.]

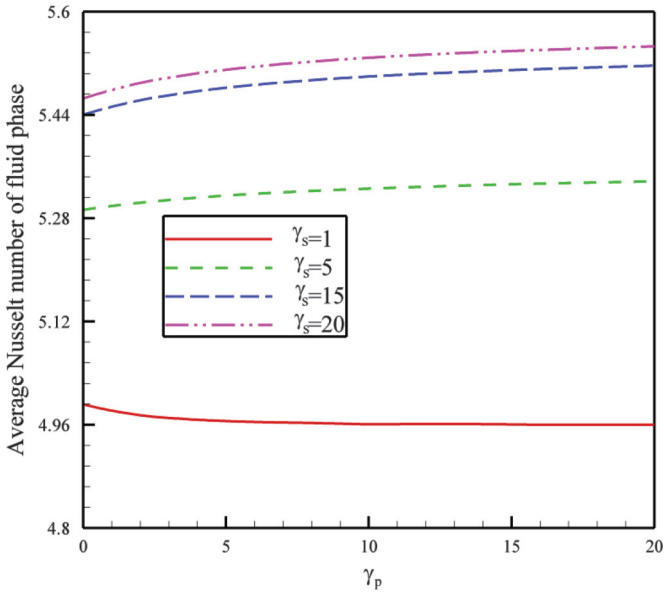

Fig. 18. Average Nusselt number of solid phase ($\overline{Nu}_s$) as a function of modified thermal capacity ratio of nanoparticles (γ_p). [Colour online.]

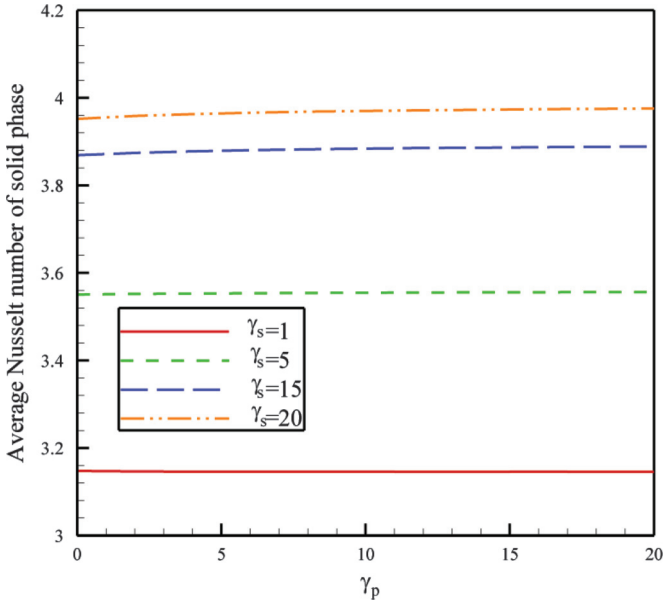

rous media (γ_s) on the average Nusselt number of the three phases. These figures depict that the addition of γ_s simultaneously increases all of the three average Nusselt numbers. Indeed, the addition of γ_s boosts the effect of the interaction of fluid and porous media at the porous medium side and tends to more effectively remove the heat from the wall and distribute it in the solid and nanoparticle phases.

Figure 17 shows that the effect of variation of γ_p on the average Nusselt number of the fluid phase depends on the magnitude of γ_s. When γ_s is low, increasing γ_p decreases the average Nusselt number of the base fluid phase, but when γ_s is high, increasing γ_p increases the average Nusselt number. Indeed, incrementing γ_p tends to boost the effect of the interfacial interaction for the

Fig. 19. Average Nusselt number of nanoparticles ($\overline{Nu}_p$) as a function of modified thermal capacity ratio of nanoparticles (γ_p). [Colour online.]

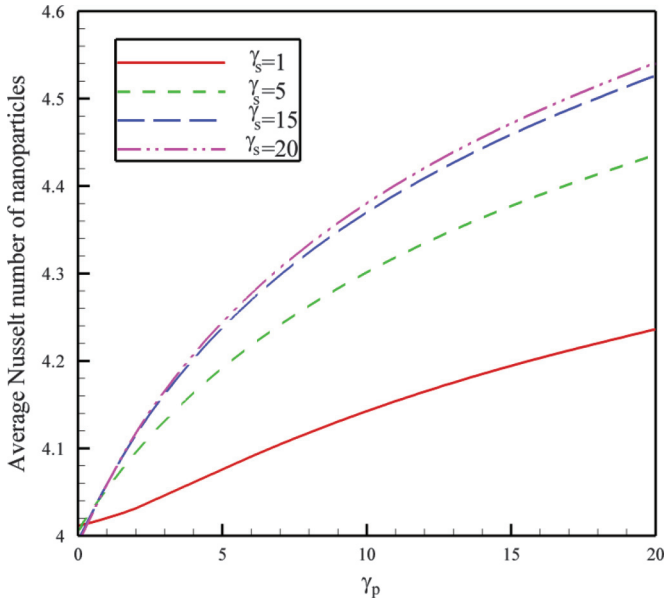

nanoparticle phase. When γ_s is small (about unity), the temperature of the fluid phase is under the strong influence of the temperature distribution in the porous phase, which results in the decrease of average Nusselt number by the increase of γ_p.

Figure 18 depicts that the addition of γ_p shows an insignificant effect on the average Nusselt number of the porous phase. This is because the variation of γ_p would directly affect the temperature profiles of the base fluid and nanoparticles, but it induces an indirect effect on the temperature profiles of the porous phase through alteration of the base fluid phase temperature.

As mentioned, the increment of γ_p would boost the interaction between the nanoparticle phase and the base fluid, and this interaction effect is much more significant on the thermal energy of the nanoparticle phase. Therefore, as seen in Fig. 19, the increment of γ_p illustrates a significant increase in the average Nusselt number of nanoparticles phase. Figure 19 also shows a focal point for very small values of γ_p, which do not have practical application at this point for nanofluid heat transfer because the values of γ_p for nanofluids are currently very high (order of 10).

Figures 20–22 depict the average Nusselt number of different phases as a function of γ_s for various values of γ_p. These figures, in agreement with the previous figures, show that the increment of γ_s is significant for all phases, but the increment of γ_p is only significant for the nanoparticle phase. Figure 20 shows a focal point (region) for average Nusselt number of the base fluid phase, which occurs for γ_s about $\gamma_s = 2.5$. This point could be of practical application as the value of $\gamma_s = 2.5$ is possible for nanofluids when the thermal conductivity of the porous matrix is low or the porosity of the porous medium is high. Figure 22 also shows that the increase of γ_p always increases the average Nusselt number for the nanoparticle phase. Figure 20 shows that the increase of γ_p (the modified heat capacity ratio for nanoparticles) starts to increase the average Nusselt number in the base fluid phase when γ_s is higher than unity. Thus, it could be concluded that for γ_s values higher than 2.5, the increase of γ_p could boost the average Nusselt numbers for both phases of base fluid and nanoparticles. However, the alteration of γ_p does not show significant effect on the average Nusselt number of the porous phase. Figure 21 also indicates that the effect of γ_p on the average Nusselt is very smooth

Fig. 20. Average Nusselt number of fluid phase ($\overline{Nu}_f$) in several modified thermal capacity ratio of nanoparticles (γ_p) as a function of modified thermal conductivity ratio of porous phase (γ_s). [Colour online.]

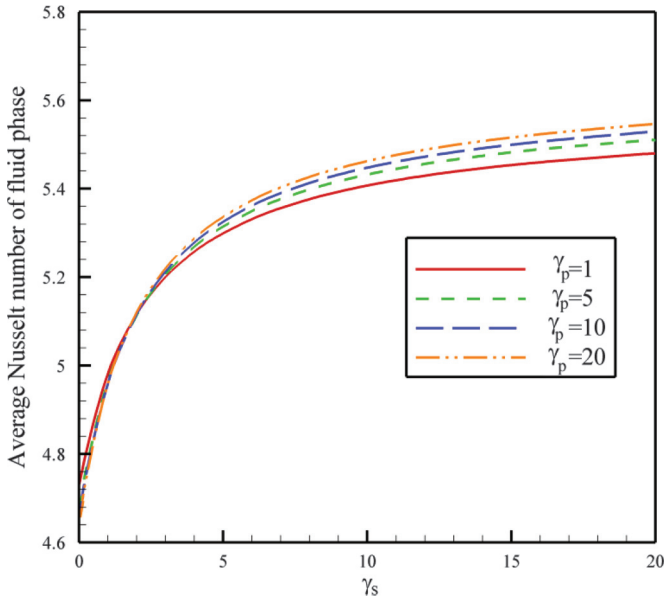

Fig. 21. Average Nusselt number of solid porous media ($\overline{Nu}_s$) in several modified thermal capacity ratio of nanoparticles (γ_p) as a function of modified thermal conductivity ratio of porous phase (γ_s). [Colour online.]

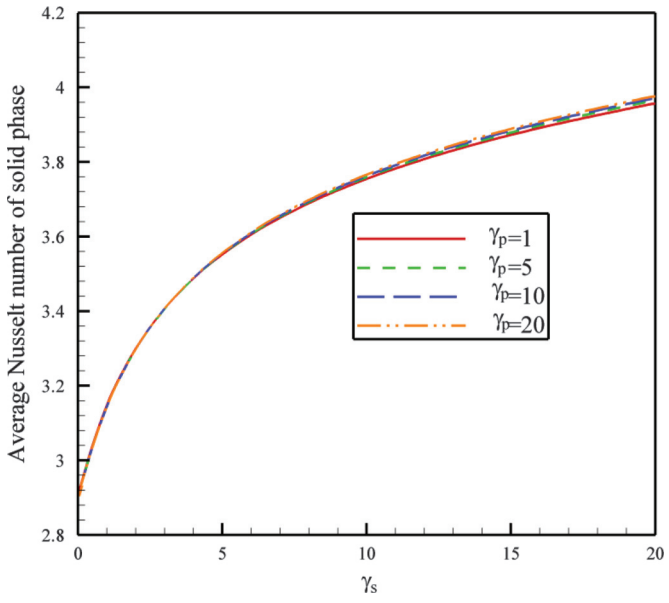

because alteration of γ_p indirectly affects the solid porous matrix through the alteration of the base fluid phase. It should be noted that the increase of interaction between the base fluid and porous medium (γ_s) significantly increases the average Nusselt number of the porous phase.

5. Conclusion

The free convective heat and mass transfer of nanofluids in a triangular cavity filled with a saturated porous medium was theoretically analyzed. There was a flush heater mounted on a part of the vertical wall while the inclined wall was kept cold. A local thermal non-equilibrium model, incorporating the three heat equation model, was employed for thermal energy of three phases of base fluid, nanoparticle, and the porous medium. The drift flux of the nanoparticle phase was modeled by using Buongiorno's nanofluid model, incorporating Brownian motion and thermophoresis effects. The governing equations were transformed into non-dimensional form, and have been solved using the finite element method. The main outcomes of the present study can be summarized as follows:

1. As the buoyancy ratio increases, the average Nusselt number for the fluid phase decreases, for the porous phase increases, and for the nanoparticle phase first increases and then decreases.
2. As the Rayleigh number increases, the average Nusselt number for the base fluid rapidly increases, but the average Nusselt number of the porous phase is almost independent of the variation of Rayleigh number. The nanoparticle phase follows the behavior of the base fluid phase, but with a smoother slope.
3. The increase of the modified conductivity ratio parameter (γ_s) enhances the average Nusselt number of all three phases, simultaneously. However, an increase of the heat capacity ratio (γ_p) would solely induce a significant enhancement on the average Nusselt number of the nanoparticle phase.
4. The augmentation of the heater size results in better heat transfer as it increases the average Nusselt number for all three phases simultaneously.
5. The increase of the aspect ratio of the enclosure reduces the average Nusselt number of all three phases. Hence, the enclosures with a low aspect ratio could result in a higher heat transfer rate.

Fig. 22. Average Nusselt number of nanoparticles ($\overline{Nu}_p$) in several modified thermal capacity ratio of nanoparticles (γ_p) as a function of modified thermal conductivity ratio of porous media (γ_s). [Colour online.]

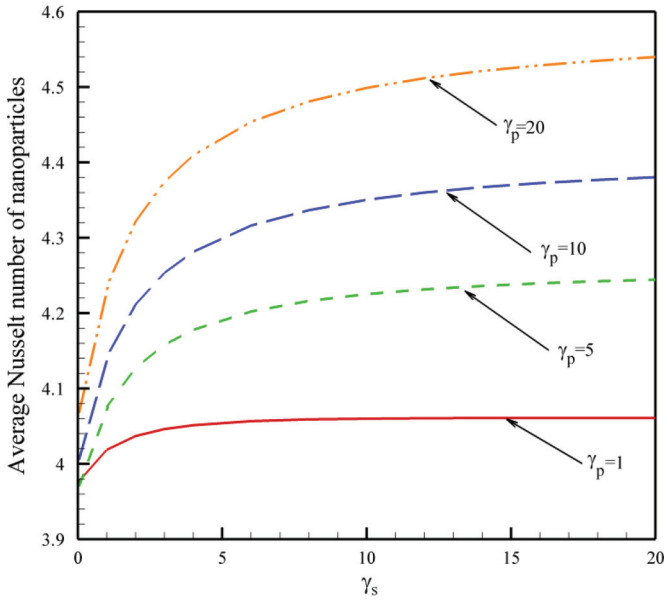

Acknowledgement

The authors acknowledge the financial support of Dezful Branch, Islamic Azad University, Dezful, Iran, and Iran Nanotechnology Initiative Council (INIC) for the financial support of the present study. The authors are tankful to Sheikh Bahaei National High Performance Computing Center (SBNHPCC) for providing computational resources, supported by the scientific and technological department of the presidential office and Isfahan University of Technology (IUT). The authors appreciate the very competent reviewers for their careful revision of the present study.

References

1. A.C. Baytas and I. Pop. Int. J. Heat Mass Transf. **42**, 1047 (1999). doi:10.1016/S0017-9310(98)00208-7.
2. N. Saeid and I. Pop. J. Porous Media **8**, 55 (2005). doi:10.1615/JPorMedia.v8.i1.50.
3. T. Basak, S. Roy, T. Paul, and I. Pop. Int. J. Heat Mass Transf. **49**, 1430 (2006). doi:10.1016/j.ijheatmasstransfer.2005.09.018.
4. T. Basak, S. Roy, and A.J. Chamkha. Int. Commun. Heat Mass Transf. **39**, 657 (2012). doi:10.1016/j.icheatmasstransfer.2012.03.022.
5. M. Sathiyamoorthy, T. Basak, S. Roy, and I. Pop. Int. J. Heat Mass Transf. **50**, 1892 (2007). doi:10.1016/j.ijheatmasstransfer.2006.10.010.
6. A.J. Chamkha and M.A. Ismael. Numerical Heat Transfer, Part A, **65**, 1089 (2014). doi:10.1080/10407782.2013.851560.
7. A.J. Chamkha and M.A. Ismael. Numer. Heat Transf. Part A: Appl. **63**, 144 (2013). doi:10.1080/10407782.2012.724327.
8. D.B. Ingham and I. Pop (Eds). Transport phenomena in porous media III. Elsevier, Oxford. 2005.
9. K. Vafai (Ed.). Handbook of porous media. CRC Press. 2005.
10. D.A. Nield and A. Bejan. *In* Convection in porous media. Springer, New York, pp. 1–29. 2013.
11. G. Huminic and A. Huminic. Renew. Sustain Energy Rev. **16**, 5625 (2012). doi:10.1016/j.rser.2012.05.023.
12. R. Saidur, K.Y. Leong, and H.A. Mohammad. Renew. Sustain. Energy Rev. **15**, 1646 (2011). doi:10.1016/j.rser.2010.11.035.
13. A. Malvandi, D. Ganji, and A. Malvandi. Int. J. Sediment Res. **29**, 423 (2014). doi:10.1016/S1001-6279(14)60056-1.
14. A. Malvandi. J. Magn. Magn. Mater. **406**, 95 (2016). doi:10.1016/j.jmmm.2016.01.008.
15. I. Mustafa, T. Javed, and A. Majeed. Can. J. Phys. **93**, 1365 (2015). doi:10.1139/cjp-2014-0689.
16. M.F. Iqbal, K. Ali, and M. Ashraf. Can. J. Phys. **93**, 290 (2014). doi:10.1139/cjp-2014-0243.
17. K. Kumar and S. Bandari. Can. J. Phys. **92**, 1703 (2014). doi:10.1139/cjp-2013-0508.
18. M.M. Rashidi, N. Freidoonimehr, A. Hosseini, O. Anwar Bég, and T.K. Hung. Meccanica, **49**, 469 (2014). doi:10.1007/s11012-013-9805-9.
19. M.M. Rashidi, A. Hosseini, I. Pop, S. Kumar, and N. Freidoonimehr. Appl. Math. Mech. **35**, 831 (2014). doi:10.1007/s10483-014-1839-9.
20. Q. Sun and I. Pop. Int. J. Therm. Sci. **50**, 2141 (2011). doi:10.1016/j.ijthermalsci.2011.06.005.
21. M.A. Sheremet, T. Grosan, and I. Pop. Transp. Porous Media, **106**, 595 (2015*a*). doi:10.1007/s11242-014-0415-3.
22. M.A. Sheremet, S. Dinarvand, and I. Pop. Phys. E: Low-dimens. Syst. Nanostruct. **69**, 332 (2015*b*). doi:10.1016/j.physe.2015.02.005.
23. M. Ghalambaz, M.A. Sheremet, and I. Pop. PlOS ONE, **10**, 1 (2015). doi:10.1371/journal.pone.0126486.
24. M.A. Sheremet and I. Pop. Transp. Porous Media, **105**, 411 (2014*a*). 10.1007/s11242-014-0375-7.
25. J. Buongiorno. J. Heat Transf. **128**, 240 (2006). doi:10.1115/1.2150834.
26. M.A. Sheremet, T. Groşan, and I. Pop. J. Heat Transf. **136**, 082501 (2014). doi:10.1115/1.4027355.
27. M.A. Sheremet and I. Pop. Int. J. Num. Methods Heat Fluid Flow **25**, 1138 (2014*b*). doi:10.1108/HFF-06-2014-0181.
28. A.V. Kuznetsov and D.A. Nield. Transp. Porous Media, **83**, 425 (2010). doi:10.1007/s11242-009-9452-8.
29. A.V. Kuznetsov and D.A. Nield. Int. J. Heat Mass Transf. **65**, 682 (2013). doi:10.1016/j.ijheatmasstransfer.2013.06.054.
30. D.A. Nield and A.V. Kuznetsov. Int. J. Heat Mass Transf. **52**, 5792 (2009). doi:10.1016/j.ijheatmasstransfer.2009.07.024.
31. D.A. Nield and A.V. Kuznetsov. Int. J. Heat Mass Transf. **68**, 211 (2014). doi:10.1016/j.ijheatmasstransfer.2013.09.026.
32. D.Y. Tzou. J. Heat Transfer **130**, 072401 (2008*a*). doi:10.1115/1.2908427.
33. D.Y. Tzou. Int. J. Heat Mass Transf. **51**, 2967 (2008*b*). doi:10.1016/j.ijheatmasstransfer.2007.09.014.
34. P. Vadász (Ed.). Emerging topics in heat and mass transfer in porous media: from bioengineering and microelectronics to nanotechnology. Springer, the Netherlands. 2008. doi:10.1007/978-1-4020-8178-1.
35. S. Rao. The finite element method in engineering. Butterworth-Heinemann. 2005.
36. P. Wriggers. Nonlinear finite element methods. Springer Science and Business Media. 2008.
37. P.R. Amestoy, I.S. Duff, and J.Y. L'Excellent.. Comput. Methods Appl. Mech. Eng. **184**, 501 (2000). doi:10.1016/S0045-7825(99)00242-X.
38. A.C. Baytas and I. Pop. Int. J. Therm. Sci. **41**, 861 (2002). doi:10.1016/S1290-0729(02)01379-0.
39. A.J. Chamkha, M.A. Mansour, and S.E. Ahmed. Heat Mass Transf. **46**, 757 (2010). doi:10.1007/s00231-010-0622-6.
40. V.A.F. Costa. Int. J. Heat Mass Transf. **47**, 2699 (2004). doi:10.1016/j.ijheatmasstransfer.2003.11.031.
41. S. Gross and A. Reusken Numerical methods for two-phase incompressible flows. Springer Science and Business Media, **40** (2011).
42. H. Zargartalebi, A. Noghrehabadi, M. Ghalambaz, and I. Pop. Transp. Porous Media **107**, 153 (2015). doi:10.1007/s11242-014-0430-4.
43. A. Behseresht, A. Noghrehabadi, and M. Ghalambaz. Chem. Eng. Res. Des. **92**, 447 (2014). doi:10.1016/j.cherd.2013.08.028.
44. A. Noghrehabadi, M. Ghalambaz, and A. Ghanbarzadeh. J. Mech. **30**, 265 (2014). doi:10.1017/jmech.2013.61.
45. M. Ghalambaz and A. Noghrehabadi. J. Comput. Appl. Res. Mech. Eng. **3**, 113 (2014).
46. B.S. Bhadauria and S. Agarwal. Transp. Porous Media, **88**, 107 (2011). doi:10.1007/s11242-011-9727-8. 10.1007/s11242-010-9613-9.
47. C. Beckermann, R. Viskanta, and S. Ramadhyani. Numer. Heat Trans. **10**, 557 (1986). doi:10.1080/10407788608913535.
48. R. Gross, M.R. Bear and C.E. Hickox. *In* Proc. 7th IHTC, San Francisco, CA. 1986.
49. D.M. Manole and J.L. Lage. *In* Heat mass transfer porous media, ASME Conference, **105** (1992).
50. S.L. Moya, E. Ramos, and M. Sen. Int. J. Heat Mass Transf. **30**, 741 (1987). doi:10.1016/0017-9310(87)90204-3.
51. A. Bejan. Lett. Heat Mass Transf. **6**, 93 (1979). doi:10.1016/0094-4548(79)90001-8.
52. K.L. Walker and G.M. Homsy. J. Fluid Mech. **87**, 449 (1978). doi:10.1017/S0022112078001718.

List of symbols

AR	aspect ratio
C	nanoparticle volume fraction
D_B	Brownian diffusion coefficient (m^2/s)
D_T	thermophoretic diffusion coefficient (m^2/s)
$\boldsymbol{g}$	gravitational acceleration vector (m/s^2)
h	height of heater (m)
H	height of cavity (m)
H_H	non dimensional height of heater
h_{fp}	interface heat transfer coefficients between the fluid and particle phases (W/m^3K)
h_{fs}	interface heat transfer coefficients between the fluid and solid-matrix phases (W/m^3K)
K	permeability of the porous medium
k	effective thermal conductivity (W/mK)
L	length of cavity (m)
Le	Lewis number
Nb	Brownian motion parameter
Nhp	Nield number for the fluid/nanoparticle interface (fluid and nanoparticle interface parameter)
Nhs	Nield number for the fluid/solid-matrix interface (fluid and solid-matrix interface parameter)
Nr	buoyancy ratio parameter
Nt	thermophoresis parameter
Nu	local Nusselt number
$\overline{\text{Nu}}$	average Nusselt number
p	pressure (atm)
Ra	thermal Rayleigh–Darcy number $\text{Ra} = (1-C_0)gK\rho_{f0}\beta(T_h - T_L)H/(\alpha_f\mu)$
Sh	local Sherwood number
T	nanofluid temperature (K)
T_c	temperature at the tilted wall (K)
T_h	temperature at the left wall (K)
$\boldsymbol{V}$	Darcy velocity (m/s)
$\bar{x}, \bar{y}$	Cartesian coordinates (m)
$\bar{u}, \bar{v}$	the velocity components along $\bar{x}, \bar{y}$ directions (m/s)
y_p	dimensional position of heater center
Y_p	dimensionless position of heater center (m)
α	effective thermal diffusivity (m^2/s)
β	thermal expansion coefficient (1/K)
γ_p	modified thermal capacity ratio for nanoparticles
γ_s	modified thermal conductivity ratio for porous phase
ε	porosity
ε_p	modified thermal diffusivity ratio for nanoparticles
θ	non-dimensional temperature
μ	dynamic viscosity (kg/ms)
ρ	fluid density (kg/m^3)
(ρc)	effective heat capacity (J/m^3K)
τ	parameter defined by $\tau = (\rho c)_p/(\rho c)_f$
ψ	non-dimensional stream function
$\overline{\psi}$	stream function (m^2/s)

Subscripts

0	ambient property
f	base fluid phase
p	nanoparticle phase
s	porous medium solid-matrix phase